# Electromagnetic properties of periodic multilayers of ultrathin metallic films from dc to ultraviolet frequencies

**Harry Contopanagos and Eli Yablonovitch**

*Department of Electrical Engineering, University of California Los Angeles, Los Angeles, California 90095*

**Nicolaos G. Alexopoulos**

*Department of Electrical and Computer Engineering, University of California Irvine, Irvine, California 92697*

Received October 5, 1998; accepted January 26, 1999; revised manuscript received March 24, 1999

Ultrathin metallic films have an interesting electromagnetic behavior as the frequency of the incident field is varied over several orders of magnitude, because of the dramatic dispersion exhibited by the metal permittivity. We study a finite multilayer of periodically placed planar conducting films for frequencies varying from the dc limit to the far ultraviolet. We provide the optimized reflectivity and transmittivity of the system for the various frequency regimes involved. Further, we produce the dispersion diagrams of the corresponding photonic bandgap structures, which clearly show the transition of the system from a metallic (low frequencies) to a dielectric (optical frequencies) behavior. In addition, simple design formulas for maximum reflectivity of finite film number $N$ are presented in terms of film thickness and film spacing in each of the representative frequency ranges. © 1999 Optical Society of America [S0740-3232(99)00808-X]

*OCIS codes:* 310.6860, 290.4210, 220.4830, 230.1480, 260.3910.

## 1. INTRODUCTION

Metallic conductors are excellent reflectors at microwave frequencies but become transparent at optical frequencies.[1] This highly dispersive behavior is well described by the permittivity given by the classical Drude model.[1] This model is a special case of a Lorentzian, where the electron oscillators have become free charge carriers. An important issue is whether one can enhance this dispersive behavior of bulk metals by using coherence effects resulting from appropriate design of thin films[2] periodically placed on dielectric substrates. This is a subject that can be examined separately in the microwave[3] and the optical[4,5] regime, because the metal permittivity behaves very differently in each of these frequency regions. According to the frequency regime, the multiple Fabry–Perot resonances that are due to periodicity[6] will be superimposed on the inherent dispersion of the material, yielding a variety of filter responses. The purpose of this paper is to examine the general filter response of such structures, optimizing both the reflection and the transmission, within the natural frequency regimes that characterize the bulk behavior of the metal.

It has already been shown that, in the microwave regime, one can increase the very high reflectivity of bulk metal by appropriate design of ultrathin-metal-film multilayers, whose individual thickness is much smaller than the skin depth at those frequencies.[3] The reflectivity enhancement is produced by correctly distributing the induced currents on *all* metal films, so that they create minimum resistive losses. It has been shown that this is a sensitive optimization, resulting in very narrow-band designs.

In this paper we will supply a unified description of this behavior and, most importantly, its evolution at optical frequencies through dispersion diagrams. This will also describe how the maximum possible reflectivity develops as the frequency increases. Our unified results will be useful in designing optimum reflectors at any frequency of engineering interest as well as optical filters in the transparency regime above the plasma frequency.

## 2. REFLECTION AND TRANSMISSION THROUGH A PERIODIC FILTER CONSISTING OF $N$ METAL FILMS

Consider the system of $N$ metal films, laterally infinite, each of thickness $d_c$, with successive films separated by a dielectric of thickness $d_d$ ($d_a$ for air gaps), as in Fig. 1. Using standard transfer-matrix theory,[7] we can derive closed-form, exact analytical expressions for the reflection and transmission coefficients of the structure under plane-wave incidence.[3]

Denoting the polarization state of the incident plane wave by $p$ ($p = 1 \rightarrow$ TE incidence, $p = 2 \rightarrow$ TM incidence) and the angle of incidence by $\theta$, we can write

$$\Gamma_N^p(\theta) = \frac{2u_{21}(1 - \xi^N)}{(u_{11} - u_{22})(1 - \xi^N) + \zeta(u_{11} + u_{22})(1 + \xi^N)}, \tag{1}$$

where

$$\zeta = \frac{u_{11} - u_{22}}{u_{11} + u_{22}}\left[1 + \frac{4u_{12}u_{21}}{(u_{11} - u_{22})^2}\right]^{1/2}, \qquad \xi = \frac{1 - \zeta}{1 + \zeta}. \tag{2}$$

0740-3232/99/092294-13$15.00 

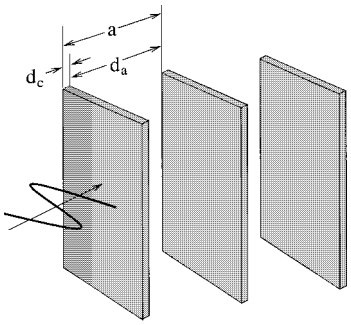


Fig. 1. Plane-wave incidence on a multilayer of metal films.

The matrix elements $u_{ij}$ are obtained from the transfer matrix $\mathbf{U}$ through one unit cell of the filter:

$$\mathbf{U} = v \times \mathbf{u},$$

$$\mathbf{u} = \begin{bmatrix} 1 - \Gamma^{1;p}_{a,c}\Gamma^{1;p}_{a,d} & -(\Gamma^{1;p}_{a,d} + \Gamma^{1;p}_{a,c}Z^{p}_{a,d}) \\ \Gamma^{1;p}_{a,c} + \Gamma^{1;p}_{a,d}Z^{p}_{a,c} & -\Gamma^{1;p}_{a,c}\Gamma^{1;p}_{a,d} + Z^{p}_{a,c}Z^{p}_{a,d} \end{bmatrix}, \quad (3)$$

where

$$v = v_1 v_2,$$

$$v_j = \left[\frac{1 - (\Gamma^{p}_{a,j})^2 \exp(-2\gamma_j d_j)}{1 - (\Gamma^{p}_{a,j})^2}\right]\exp(\gamma_j d_j), \qquad j = 1, 2, \quad (4)$$

and the functions $\Gamma^{1;p}_{a,j}$ are the reflection coefficients of one slab of material $j \in \{\text{conductor} \equiv c,\ \text{dielectric} \equiv d\}$ for $p$-polarized plane-wave oblique incidence from air, given by

$$\Gamma^{1;p}_{a,j} = \Gamma^{p}_{a,j}\left[\frac{1 - \exp(-2\gamma_j d_j)}{1 - (\Gamma^{p}_{a,j})^2 \exp(-2\gamma_j d_j)}\right], \quad (5)$$

and the $Z^{p}_{a,j}$ are closely related (but irreducible) functions, given by

$$Z^{p}_{a,j} = \frac{-(\Gamma^{p}_{a,j})^2 + \exp(-2\gamma_j d_j)}{1 - (\Gamma^{p}_{a,j})^2 \exp(-2\gamma_j d_j)}. \quad (6)$$

In these equations appear the intrinsic (bulk) reflection coefficients of the materials, $\Gamma^{p}_{a,j}$, and the propagation constants $\gamma_j$ for the plane waves:

$$\Gamma^{p=1}_{a,j} = \frac{(\eta_j/\cos\theta_j) - (1/\cos\theta)}{(\eta_j/\cos\theta_j) + (1/\cos\theta)},$$

$$\Gamma^{p=2}_{a,j} = \frac{\eta_j \cos\theta_j - \cos\theta}{\eta_j \cos\theta_j + \cos\theta},$$

$$\gamma_j = jk_0 n_j \cos\theta_j, \quad (7)$$

where $\eta_j$ are the relative wave impedances and $n_j$ are the refractive indices. For nonmagnetic materials, which we will be using in this paper,

$$n_j = \frac{1}{n_j}, \qquad n_j = \sqrt{\epsilon_j}, \quad (8)$$

and, from Snell's law,

$$\cos\theta_j = (1 - \eta_j^2 \sin^2\theta)^{1/2}. \quad (9)$$

The transmission coefficient through the filter, $T^{p}_{N}(\theta)$, is similarly calculated:

$$T^{p}_{N}(\theta) = \Gamma^{p}_{N}(\theta)\left(\frac{u_{11} + u_{22}}{u_{21}}\right) \times \zeta\left[\frac{2\Gamma^{1;p}_{a,c}\Gamma^{1;p}_{a,d}\exp(-\gamma_c d_c)\exp(-\gamma_d d_d)}{\Gamma^{p}_{a,c}\Gamma^{p}_{a,d}(u_{11} + u_{22})(1 + \zeta)}\right]^N \times (1 - \xi^N)^{-1}. \quad (10)$$

These formulas are exact, and the behavior of the system is completely determined once the complex permittivity functions $\epsilon_c$, $\epsilon_d$ are specified. It is important to note that the dispersive behavior of $\Gamma_N$, $T_N$ derives from two sources:

1. The coherence that is due to periodicity. This property resides in the phase factors $\exp(\gamma_j d_j)$, which produce Fabry–Perot scaling with scale $k_0 n_j(\omega) d_j$. We note that, for dispersive bulk media, the corresponding refractive indices $n_j$ are already frequency dependent; therefore the above Fabry–Perot scaling deviates from the usual one $(k_0 d_j)$ for nondispersive media.
2. The dispersion that is due to the bulk reflection coefficients $\Gamma^{p}_{a,j}(\omega)$. These depend on the wave impedances $\eta_j$, which are clearly dispersive, but do not depend on the thicknesses.

The combined effect of sources 1 and 2 can create several different filtering options, especially in the plasma frequency regime, where $\Gamma_c$ exhibits the transparency transition. We further note that, although our system is simple geometrically, a complete examination and optimization of its parameter and frequency dependence is nontrivial. Even for nondispersive permittivities for the materials $(\epsilon_j = \epsilon_j^r - j\epsilon_j^i)$, the system's reflection and transmission depend on seven parameters $(N, d_c, d_d, \epsilon_c^r, \epsilon_c^i, \epsilon_d^r, \epsilon_d^i)$ and the frequency $\omega$. What we will do is systematically optimize the system's response in a way that makes the physical scaling of those variables apparent, and so the conclusions derived are numerically valid without specifying concrete materials and fixed optical constants.

## 3. NUMBER OF FILMS $N \to \infty$

The eigenvalues $w_{1,2}$ of the unit-cell matrix $\mathbf{U}$ provide the Bloch–Floquet propagation constant for the medium composed of an infinite number of metal films $(N \to \infty)$:

$$\exp[\pm jk(d_c + d_a)] = w_{1,2} = \frac{\mathrm{Tr}(\mathbf{U}) \pm \{[\mathrm{Tr}(\mathbf{U})]^2 - 4\,\mathrm{Det}(\mathbf{U})\}^{1/2}}{2} = \frac{v(u_{11} + u_{22})(1 \pm \zeta)}{2}. \quad (11)$$

One can show, after some tedious algebra, that $\mathrm{Det}(\mathbf{U}) = 1$, and hence the two eigenvalues are inverses of each other and correspond to left/right propagation of the Floquet modes inside the structure. Since we have metallic films, which are lossy at all frequencies, there is

always absorption, and hence the system has stop bands at all frequencies. Therefore $\exp[jk(d_c + d_a)]$ has to be identified with the eigenvalue whose modulus is $> 1$, which happens to be

$$w \equiv w_1 = \frac{v(u_{11} + u_{22})(1 + \zeta)}{2}. \tag{12}$$

Therefore, separating $k = k^r - jk^i$ and writing the total thickness of the unit cell as $a \equiv d_c + d_d$, we obtain the attenuating part of the Bloch–Floquet propagation constant by

$$k^i a = \ln\left|\frac{v(u_{11} + u_{22})(1 + \zeta)}{2}\right|. \tag{13}$$

It is important to note that the above expression provides the total attenuation of the wave as it propagates down the structure. This amount of attenuation is adjustable, because it depends irreducibly on both the coherence effect of the photonic bandgap (PBG) and the material dispersion, namely, on $d_d$, $d_c$, and $\omega$, which enter the functions $v$, $u_{ij}$, and $\zeta$ above. For a given $d_c$ and $d_d$, the induced currents inside the conductor and the dielectric produce a certain amount of resistive loss, which, however, can be adjusted by varying these thicknesses. This adjustment affects the induced currents and, as we will see below, produces resonances in the total attenuation, which will actually be the most important part of the dispersion diagrams.

Another point that we wish to make, which is not often mentioned, is that the above propagation constant is an exact solution for the semi-infinite medium ($N \to \infty$), filling up the half-space $z > 0$, not just for an infinite medium. This is conceptually important because it allows us to clearly separate the excitation region $z < 0$ from the PBG medium region $z > 0$ and even to choose excitations different from the plane waves that we present in this paper (e.g., line or dipole excitations). This is easily seen by computing the eigenvectors of **U** and showing that the field incident on the semi-infinite structure and a reflected field with reflection coefficient

$$\Gamma_\infty = \frac{U_{21}}{w - U_{22}} = \frac{vu_{21}}{w - cz} = \frac{2u_{21}}{u_{11} - u_{22} + \zeta(u_{11} + u_{22})} \tag{14}$$

form such an eigenvector.

The reflection coefficient in Eq. (14), on the other hand, can be derived from the finite-$N$ reflection coefficient, obtained from Eq. (1) directly, by observing that

$$\xi \equiv \frac{1 - \zeta}{1 + \zeta} = \exp(-2jka) \to |\xi| < 1 \tag{15}$$

and hence that

$$\lim_{N=\infty} \Gamma_N^p = \frac{2u_{21}}{u_{11} - u_{22} + \zeta(u_{11} + u_{22})}, \tag{16}$$

which is identical with $\Gamma_\infty$ of Eq. (14), and thus the proof is completed.

In the rest of this paper, we will present results for the choice of air as the dielectric between metal films and for normal plane-wave incidence only. Important dispersive effects come from the metal rather than the dielectric; therefore this will simplify the parameter dependence without affecting the physical description or any of our general conclusions. It will only mildly affect specific responses quantitatively in comparison with realistic designs, where dielectric substrates would have to be used to support the thin metal films.[8] In that case one can repeat our analysis, using our above formulas and simply substituting the permittivity of the desired dielectric. Note that when the dielectric is chosen to be air, the formulas in Eqs. (1)–(7) simplify, since $\Gamma_{a,d}^p = \Gamma_{a,d}^{1;p} = 0$, $Z_{a,d}^p = \exp(-2\gamma_a d_a)$.

## 4. SCALED PARAMETERIZATION OF PHASE SHIFTS

It is important to study the above system in a way largely independent of the precise values for $\omega_p$ and $\gamma$ that one uses for any particular metal. Further, since we wish to explore a large range of frequencies extending over 16 orders of magnitude, the thicknesses of the metal films and the air gaps should be parameterized in a natural way that accounts easily for the scaling of the system with frequency.

An excellent model for the metal permittivity is the Drude model:

$$\epsilon_c = 1 - \frac{{\omega_p}^2}{\omega(\omega - j\gamma)}, \tag{17}$$

where, for most metals, the permittivity parameters are in the range

$$7 \text{ eV} < \frac{h\omega_p}{2\pi} < 15 \text{ eV}, \qquad 0.05 \text{ eV} < \frac{h\gamma}{2\pi} < 0.13 \text{ eV} \tag{18}$$

and result from fits to somewhat model-dependent and surface-preparation-dependent reflectivity data.[1,9] For the rest of this paper, we will choose the representative values

$$\frac{h\omega_p}{2\pi} = 7 \text{ eV} \to \omega_p = 10^{16} \text{ Hz}, \qquad \gamma = 10^{-2}\omega_p. \tag{19}$$

At microwave frequencies this gives a dc conductivity

$$\epsilon(\omega \ll \gamma) \simeq 1 - j\frac{({\omega_p}^2/\gamma)}{\omega} \to \sigma = \epsilon_0\frac{{\omega_p}^2}{\gamma}$$

$$\simeq \mathcal{O}(10^7 \text{ S/m}), \tag{20}$$

which is typical of good conductors at low frequency.

The skin depth can be calculated from its definition, as a function of frequency, without approximations. Given that the refractive index of the metal is

$$n_c = \sqrt{\epsilon_c} \equiv \beta - j\alpha, \tag{21}$$

and with $k_0$ denoting the free-space wave number, the skin depth is

$$\delta(\omega) = \frac{1}{k_0\alpha}, \tag{22}$$

where we use the microwave definition of skin depth in which the damping characterizes the field amplitude. Using the Drude permittivity and the scaling parametrization

$$s_0 \equiv \frac{\omega_p}{\gamma}, \qquad s \equiv \frac{\omega}{\gamma}, \tag{23}$$

we obtain

$$\beta(s, s_0) = \frac{1}{\sqrt{2}} \left\{ \left( 1 - \frac{{s_0}^2}{1 + s^2} \right) + \left[ \left( 1 - \frac{{s_0}^2}{1 + s^2} \right)^2 + \left( \frac{{s_0}^2/s}{1 + s^2} \right)^2 \right]^{1/2} \right\}^{1/2}, \tag{24}$$

$$\alpha(s, s_0) = \frac{1}{\sqrt{2}} \frac{\dfrac{{s_0}^2/s}{1 + s^2}}{\left\{ \left( 1 - \dfrac{{s_0}^2}{1 + s^2} \right) + \left[ \left( 1 - \dfrac{{s_0}^2}{1 + s^2} \right)^2 + \left( \dfrac{{s_0}^2/s}{1 + s^2} \right)^2 \right]^{1/2} \right\}^{1/2}}. \tag{25}$$

The skin depth at all frequencies becomes

$$\delta(s, s_0) = \frac{\lambda(\gamma)}{2\pi} \frac{1}{s\alpha(s, s_0)}, \tag{26}$$

where we have used the notation for the free-space wavelength $\lambda_0 = 2\pi\omega/c \equiv \lambda(\omega)$. For our purposes a natural frequency normalization is provided by $\gamma$, which is always in the infrared (IR) range, between the dc limit and the plasma frequency. Note that, while a plot of $\delta(s, s_0)$ as a function of frequency $\omega$ (in hertz) is sensitive to the exact material parameters, as shown in Fig. 2, a plot of $\delta(s, s_0)/\lambda(\gamma)$ versus $s$ is completely insensitive to the exact choice of parameters.

The parameterization of the conductor thickness can also be done in a scalable way, which is equally natural. The phase shift produced by the metal film is

$$\gamma_c d_c = \left[ j \frac{\beta(s, s_0)}{\alpha(s, s_0)} + 1 \right] \frac{d_c}{\delta(s, s_0)}. \tag{27}$$

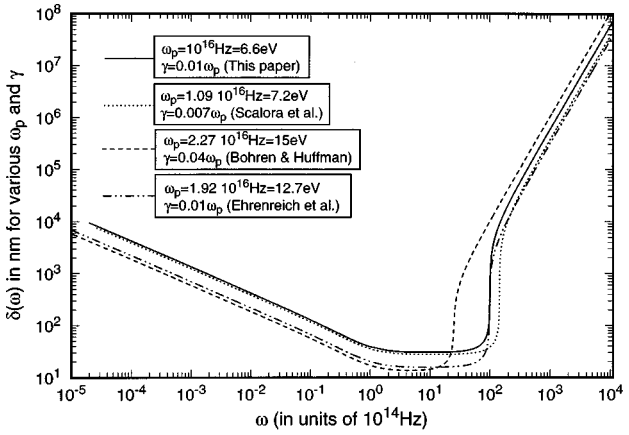


Fig. 2. Conductor skin depth versus frequency for various values of $\omega_p$, $\gamma$. The difference can be normalized away by transforming the axes as $\omega \to \omega/\gamma$, $\delta \to \delta/\lambda(\gamma)$.

From a scaling point of view, the natural parameterization is to trade off the conductor thickness dependence $d_c$ with the variable

$$x \equiv \frac{d_c}{\delta(s, s_0)}. \tag{28}$$

Similarly, the phase shift produced by the dielectric (or air-gap) thickness can be written as

$$\gamma_a d_a = j k_0 d_a = jy, \tag{29}$$

where we have introduced the other natural variable parameterizing the air-gap thickness:

$$y \equiv k_0 d_a = \frac{2\pi d_a}{\lambda(\omega)} = s \frac{2\pi d_a}{\lambda(\gamma)}. \tag{30}$$

Specifying the parameters $\omega_p$, $\gamma$ in the metal introduces one single length scale [$\lambda(\gamma)$ with our choice]. Among the three fundamental quantities $d_c, d_a, \omega$ characterizing the design of our system, varying only $y$ is equivalent to varying $d_a$, varying only $x$ is equivalent to varying $d_c$, but varying only $s(\omega)$ will affect not just the thickness-independent bulk reflection coefficient $\Gamma^p_{a,c}$ but also the parameters $x, y$ (phase shifts $\gamma_c d_c$, $\gamma_a d_a$) as well. This trivial observation is, however, important for dispersive media, as we have in our case, and is not often made, the reason being that such systems have always been systematically analyzed in a unified way not over the whole spectrum but only within specific bands, where the metal optical constants do not vary significantly.

From the above discussion it is obvious that the orthogonal cuts of the system's response functions are the frequency and the two phase shifts $\gamma_c d_c$ [Eq. (27)] and $\gamma_a d_a$ [Eq. (29)]. Of the two phase shifts, the former scales to the normalized thickness $x$ [Eq. (28)], without any extra frequency dependence, *only* for frequencies $\omega < \gamma$. We will respect this scaling accordingly in most of the plots in this paper.

## 5. DISPERSION DIAGRAMS

In this section we will present the dispersion diagrams for the semi-infinite structure ($N \to \infty$). As explained above, we will present the pairs of plots $k_0 a$ versus $\mathrm{Re}(k)a$ and $\mathrm{Im}(k)a$, respectively.

Because we have a dissipative medium, both components are necessary, especially since the latter completely determines the systematics of field penetration inside the PBG medium. We point out that we have several choices in constructing these diagrams. The Bloch–Floquet

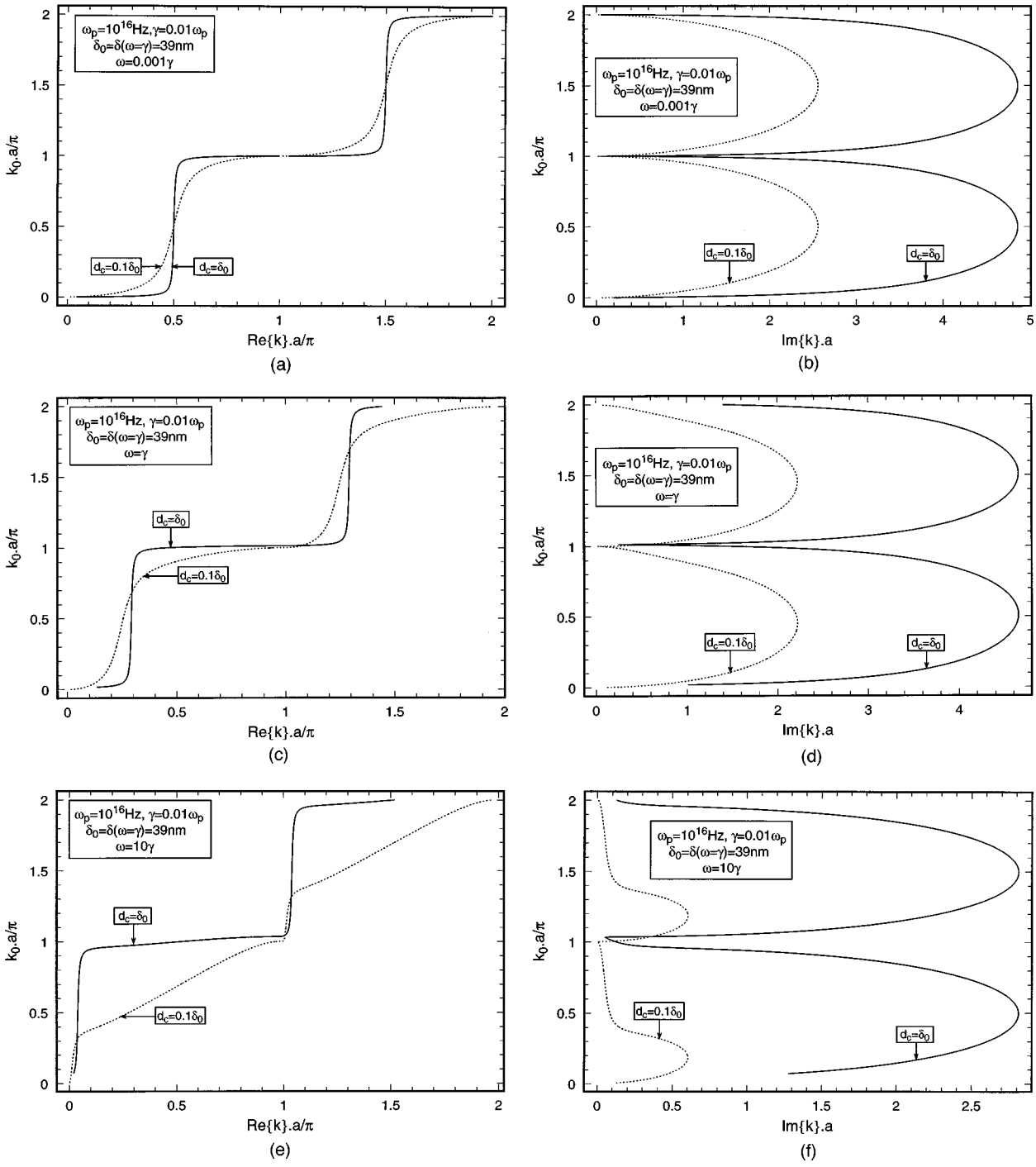


Fig. 3. Continues on next page.

propagation constant $k$ is an irreducible function of $d_c$, $d_a$, $\omega$ for fixed permittivity parameters $\omega_p$, $\gamma$. To present two-dimensional plots, one has to assume two cuts in this parameter space. In other words, two relations $f_i(d_c, d_a, \omega) = 0$, $i = 1, 2$, have to be input. Common choices would be (1) $d_c$, $d_a$ = constants, $\omega$ varies; (2) $d_c$, $\omega$ = constants, $d_a$ varies; (3) $\omega$ = constant, $d_c$ = constant $\times$ $d_a$, $d_a$ varies; etc.

Choosing option (1) would necessitate covering thousands of Brillouin zones (for fixed film spacing), since the frequency would vary over many orders of magnitude, which would affect the air-gap phase shift $y$ proportionately, or producing many dispersion diagrams, all with the same frequency variation but different film spacing chosen to resonate in specific frequency bands. We prefer option (2), which respects the separable functional dependence of the system's response, and we will scan the various frequencies $\omega$ parametrically, from the microwave to the ultraviolet (UV) regime. This option is identical with the way dispersion diagrams for PBG's made up of dispersionless materials are produced, since in those it is precisely the phase shift that is being varied and the frequency is entirely contained there. It also has the advantage of always plotting within the first few Brillouin

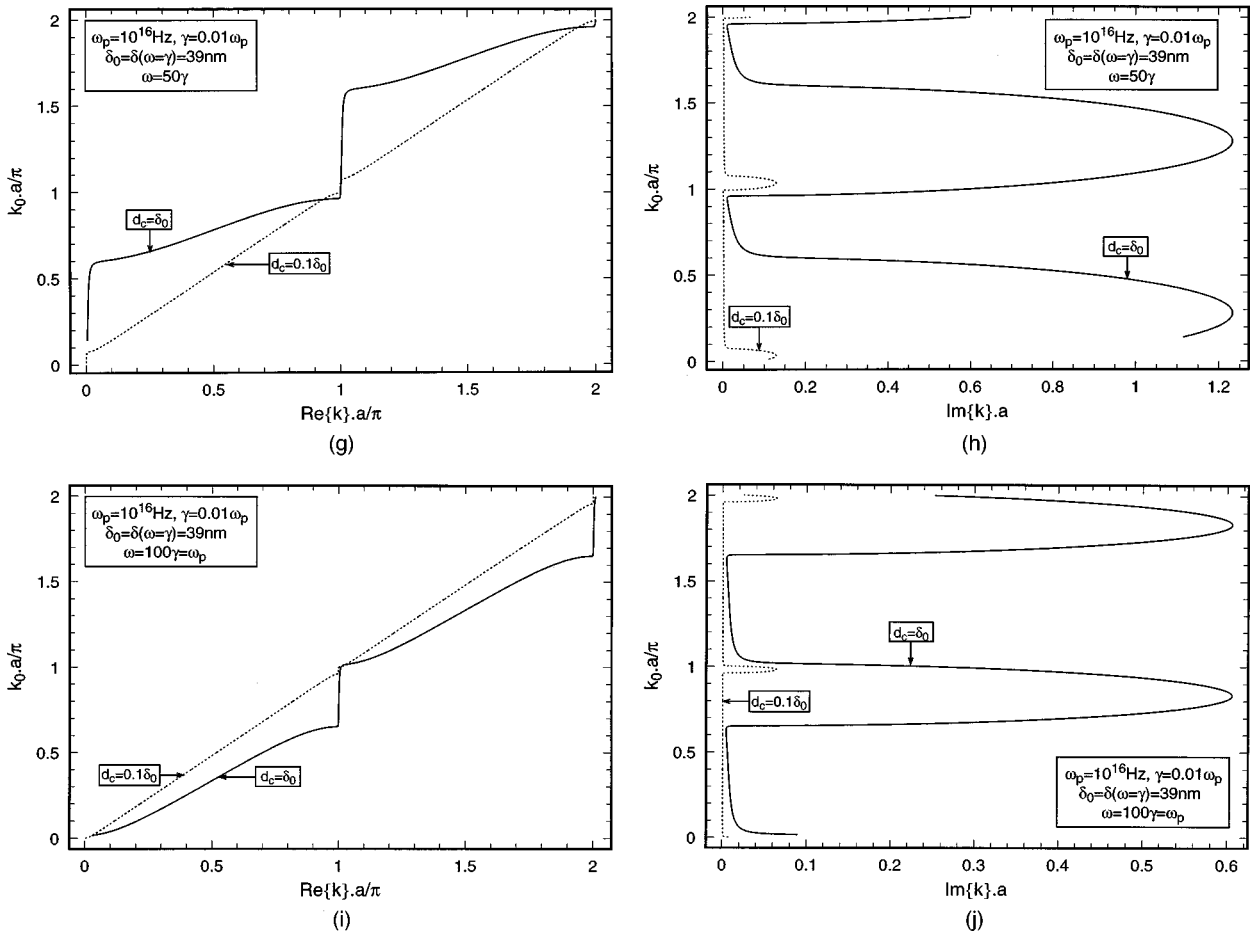


Fig. 3. Dispersion diagrams for the PBG medium: (a), (b) at $\omega = 0.001\gamma$ (microwave); (c), (d) at $\omega = \gamma$ (far IR); (e), (f) at $\omega = 10\gamma$ (near IR); (g), (h) at $\omega = 50\gamma$ (visible); (i), (j) at the plasma frequency $\omega = 100\gamma$ (near UV).

zones, while the parametric variation provides a complete description of the dispersive effects of the material on the system response. Further, for any metal thickness of interest and any frequency $\omega_p < 10\gamma$, the conventional phase shift $k_0 a$ that is always plotted in dispersion diagrams is almost entirely reproduced by the phase shift in the air gap ($k_0 d_a$), because the metal film thicknesses are tiny compared with the wavelength. To be able to compare metal thicknesses directly, as the frequency changes parametrically, we will choose the normalization standard for these thicknesses as the conductor skin depth at frequency $\omega = \gamma$:

$$d_c = x_0 \delta_0, \qquad \delta_0 \equiv \delta(s = 1, s_0), \tag{31}$$

where the parameter $x_0$ will be given fixed numerical values in the rest of this paper.

In Fig. 3 we plot the real and imaginary dispersion diagrams for parametrically varying frequencies from the microwave to the optical. We see that for $\omega \leqslant \gamma$ the dispersion plots have a very different appearance from that of the usual plots for dielectric PBG's[10]: The real parts of the plots are extremely flat near half-wavelength separation, while the imaginary plots show very large attenuation for any separation *except* near half-wavelength. There the attenuation gets close to zero. It is because the wave penetrates deeply into the structure at these regions that the reflectivity is expected to be enhanced there. This is equivalent to an optimal distribution of the induced currents, along the metal interfaces, that will ensure minimum field amplitudes inside the metal films. Indeed, it can be shown that, at these regions of $k_0 a$, the field amplitude is minimum inside the metal, while at the regions of $k_0 a$ of high attenuation, the field amplitude is maximum inside the metal. As we probe higher frequencies [Figs. 3(g)–3(j)], the dispersion diagrams undergo a transition to a low-loss dielectric PBG. The imaginary parts of the plots show a broadband lossless behavior, while the bandgaps become mostly reactive.

## 6. REFLECTIVITY MAXIMIZATION IN THE MICROWAVE REGIME

In the rest of this paper, we will present results for power reflection and transmission from the filter in specific frequency regimes of engineering interest. We start from the microwave regime, which appears, from the dispersion diagrams of Section 5, to extend all the way up to $\omega \leqslant \gamma$. In this regime the bulk reflectivity of the metal is extremely close to 100%; therefore, for computational purposes, we will quantify the reflectivity of our filter through the unloaded $Q$ factor

$$Q_N = \frac{1}{1 - |\Gamma_N|^2}, \tag{32}$$

which is really the finesse of a cavity having these filters as walls. Further, we will normalize the above quantity with respect to the intrinsic (bulk) metal $Q$ factor

$$Q_{\text{metal}} = \frac{1}{1 - |\Gamma_{a,c}|^2}, \tag{33}$$

with $\Gamma_{a,c}$ provided in Eqs. (7) (we drop the polarization superscript, since we will present only normal incidence). Apart from yielding clean plots, this parameterization provides a ratio $Q_N/Q_{\text{metal}}$ completely independent of the precise permittivity values that make up the dc conductivity $\sigma$, provided that

$$\frac{{\omega_p}^2}{\gamma\omega} \gg 1 \rightarrow \frac{{s_0}^2}{s} \gg 1, \tag{34}$$

which is the case for all except extreme-UV frequencies.

In this section we will present results as a function of metal film thickness ($d_c$) or air-gap thickness ($d_a$) for a fixed frequency, which we will choose as $\omega = 2\pi \times 5$ GHz. We point out, however, that these results are valid for *all* frequencies satisfying relation (34). To show this, we can write in this regime the phase shift inside the metal as

$$\gamma_c d_c \simeq (1 + j)x, \tag{35}$$

since

$$\frac{\beta(s, s_0)}{\alpha(s, s_0)} \simeq 1 + \mathcal{O}(s/{s_0}^2). \tag{36}$$

Similarly,

$$\Gamma_{a,c} \simeq -\left(1 - \frac{1 + j}{\Delta}\right), \qquad \Delta \equiv \sqrt{\frac{{s_0}^2}{2s}} \gg 1. \tag{37}$$

In the microwave regime the quantity ${s_0}^2/s$ is typically of the order of $10^8$. Therefore, in this regime, the variables $x$, $y$, and $s$ become completely independent. Hence all our results in this section will be valid for all microwave frequencies if they are presented in terms of the scaling variables $x$, $y$ and are normalized with respect to the intrinsic $Q$ of the bulk metal, $Q_{\text{metal}}$. The specific frequency dependence of $Q_N$, apart from the scaling variables $x$, $y$ is introduced in the very large frequency-dependent factor $\Delta$, which affects $Q_N$, $Q_{\text{metal}}$ multiplicatively (within an accuracy of eight decimals) and therefore leaves the ratio $Q_N/Q_{\text{metal}}$ invariant.

### A. Impedance of Free-Space Equivalent Thickness

We will first show the power balance of a single metal film of arbitrary thickness in the microwave regime. The results of this subsection are very similar to those of Ref. 11, especially Fig. 3 and Eq. (14) of that reference.

In Fig. 4 we see that the film becomes significantly reflecting once absorption and transmission start decreasing with thickness. The length scale that sets the critical film thickness is found at the peak of the absorption curve. This critical thickness, which we will denote by $\delta_{\text{IFSET}}$, is independent of frequency (for frequencies smaller than the near IR) and depends only on the material conductivity:

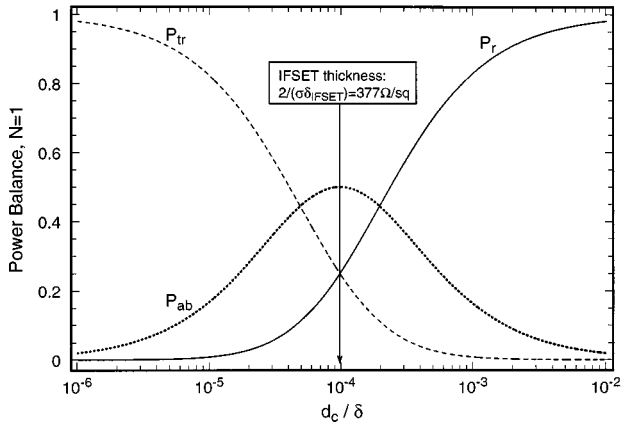


Fig. 4. Power balance of a single metal film, as a function of the film's normalized thickness in terms of its skin depth $\delta$, at frequency $\omega = 2\pi \times 5$ GHz. $P_{\text{ab}}$, $P_{\text{tr}}$, and $P_r$ refer to the absorbed, transmitted, and reflected power, respectively.

$$\delta_{\text{IFSET}} = \frac{2\epsilon_0}{\sigma\mu_0} = \frac{2\gamma}{{\omega_p}^2\mu_0}. \tag{38}$$

Therefore this is a new fundamental length scale characterizing thin-film conductors. From Eq. (38) we have chosen to call this fundamental length scale impedance of free-space equivalent thickness (IFSET), and from Fig. 2 we see that it refers to ultrathin metal films, typically in the range of nanometers, a full 3–4 orders of magnitude smaller than the conductor skin depth.

### B. Resonant Regions

For the microwave regime specifically, the attenuation caused by the metal is huge, while the intrinsic reflectivity of the metal is also very high. Therefore the resonances that minimize that attenuation are very narrow band, and their positions are very fine tuned, as is seen in Fig. 4. Hence it is useful to locate them analytically, deriving some simple design formulas along the way.

We expect these resonant regions to be at the vicinity of $y \simeq \pi \rightarrow d_a \simeq \lambda_0/2$. We will first show that such resonant behavior indeed exists, by obtaining approximate expressions for $\Gamma_\infty$. These approximations will also be useful in locating the resonant regions and providing highly accurate simplified expressions for the design of the system. Let us parameterize the resonant regions in $y$ by

$$y = \pi - \frac{\epsilon}{2}, \tag{39}$$

where $\epsilon$ is a small parameter compared with 1. Starting from the intrinsic reflection coefficient $\Gamma_{a,c}$, we can write

$$\frac{1 + j}{2\Delta} \equiv \frac{1 + j}{2}\tau\frac{\epsilon}{2} \equiv h\frac{\epsilon}{2}, \tag{40}$$

where we have parameterized the other small parameter of the problem, $1/\Delta$, in terms of $\epsilon$, i.e.,

$$\frac{1}{\Delta} = \tau\frac{\epsilon}{2}, \tag{41}$$

and $\tau$ is a multiplicative parameter, which can be $\mathcal{O}(1)$ or higher. Taylor-expanding $\Gamma_{a,c}$, $\Gamma^1_{a,c}$ up to $\mathcal{O}(\epsilon^2)$, we have

$$\Gamma_{a,c} = -\left(1 - h\epsilon + \frac{h^2}{2}\epsilon^2\right), \tag{42}$$

$$\Gamma^1_{a,c} = -\left[1 - h\frac{1+\chi}{1-\chi}\epsilon + \frac{1+\chi^2+6\chi}{2(1-\chi)^2}\epsilon^2\right], \tag{43}$$

where

$$\chi \equiv \exp[-(1+j)2x]. \tag{44}$$

The expansion of $\Gamma^1_{a,c}$ is valid only as long as $x$ is not close to zero and is very accurate up to $x \geqslant 0.1$. All our subsequent expressions will also be valid in that range of layer thicknesses. Finally,

$$Z_{a,c}Z_{a,a}(x,y) = -1 + 2\left(h\frac{1+\chi}{1-\chi} - \frac{j}{2}\right)\epsilon - 2\left(h\frac{1+\chi}{1-\chi} - \frac{j}{2}\right)^2\epsilon^2. \tag{45}$$

From these expressions we obtain

$$\left[1 - \exp(-2jy)\left(\frac{2\Gamma^1_{a,c}}{1 - Z_{a,c}Z_{a,a}}\right)\right]^{1/2} = \epsilon\left(h^2 - jh\frac{1+\chi}{1-\chi} - \frac{1}{4}\right)^{1/2} \equiv \epsilon\psi, \tag{46}$$

$$\zeta = \left(\frac{1 - Z_{a,c}Z_{a,a}}{1 + Z_{a,c}Z_{a,a}}\right)\psi\epsilon, \tag{47}$$

where, if $\epsilon > 0$, $\psi$ would be in the first Riemann sheet in order to yield $\zeta$ in the same Riemann sheet in the above equation. The $\infty$-layer reflection coefficient becomes

$$\Gamma_\infty = \frac{2\Gamma^1_{a,c}}{1-z}\frac{1}{1+\psi\epsilon} \simeq -\left[1 - \left(\psi + \frac{j}{2}\right)\epsilon + \frac{1}{2}\left(\psi + \frac{j}{2}\right)^2\epsilon^2\right]. \tag{48}$$

These expressions allow us to readily compute the $Q$ factors in closed form:

$$|\Gamma_\infty|^2 = 1 - \epsilon 2\psi_r + \epsilon^2 2{\psi_r}^2, \tag{49}$$

$$|\Gamma_{a,c}|^2 = 1 - \epsilon 2h_r + \epsilon^2 2h_r^2. \tag{50}$$

Therefore

$$\frac{Q_\infty}{Q_{\text{metal}}} = \frac{h_r}{\psi_r}\left(\frac{1 - \epsilon h_r}{1 - \epsilon\psi_r}\right), \tag{51}$$

where the $\epsilon$-dependent term may be retained if extreme accuracy is required. The real parts of $h$ and $\psi$ can be readily computed:

$$h_r = \frac{\tau}{2}, \tag{52}$$

$$\psi_r = \frac{\tau}{2}\left(\frac{R_-(x)}{\tau} - \frac{1}{2\tau^2} + \left\{\left[\frac{R_-(x)}{\tau} - \frac{1}{2\tau^2}\right]^2 + \left[\frac{R_+(x)}{\tau} - 1\right]^2\right\}^{1/2}\right)^{1/2}, \tag{53}$$

where

$$R_\pm(x) \equiv \frac{1 - \exp(-4x) \pm 2\exp(-2x)\sin 2x}{1 + \exp(-4x) - 2\exp(-2x)\cos 2x}. \tag{54}$$

The final expression for the $Q$-factor ratio is

$$\frac{Q_\infty}{Q_{\text{metal}}} \simeq \frac{1}{\left(\frac{R_-(x)}{\tau} - \frac{1}{2\tau^2} + \left\{\left[\frac{R_-(x)}{\tau} - \frac{1}{2\tau^2}\right]^2 + \left[\frac{R_+(x)}{\tau} - 1\right]^2\right\}^{1/2}\right)^{1/2}}. \tag{55}$$

The functions $R_\pm(x)$ are $\mathcal{O}(1)$ or less in the range of $x$ where these expansions are valid, and relation (55) is a form of resonance.

### C. Results for the Reflectivity-Maximized System

In Fig. 5 we plot the normalized $Q_\infty$ factor for the semi-infinite medium ($N \to \infty$) for selected values of resonant air-gap thicknesses (frequencies)

$$y_R \equiv (k_0 d_a)_R = \pi - \frac{1}{\Delta\tau}. \tag{56}$$

We observe that the resonant $Q$ factor is a monotonically decreasing function of the normalized metal film thickness, and the equation

$$\frac{Q_\infty^{\max}}{Q_{\text{metal}}} = \sqrt{\pi}\frac{\delta}{d_c} \tag{57}$$

perfectly describes all the resonances. Therefore it provides a simple formula for the maximum possible reflectivity of the semi-infinite system, made up of any good conductor at any frequency less than the IR, as a function of metal film thickness. For the important range $0.1 \leqslant d_c/\delta$, the curve of Eq. (57) can be reproduced from our formula giving $\Gamma_\infty$ at the optimized line

$$y_R(x) \equiv (k_0 d_a)_R(x) = \pi - \frac{x^{0.9965}}{\Delta}. \tag{58}$$

In Figs. 6 and 7, we examine the maximized reflectivity response of a filter composed of a variable number $N$ of metal films. Note from these curves that the scaling law

$$\left.\frac{Q_N^{\max}}{Q_{\text{metal}}}\right|_{d_c, d_a = \text{opt}} = \sqrt{N} \tag{59}$$

follows. Equations (57)–(59) together provide extremely simple formulas for the design of the system, valid for any conductor, at any frequency $\omega < \gamma$.

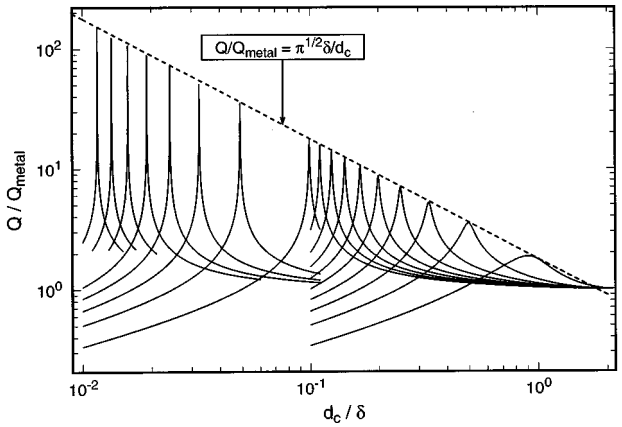


Fig. 5. Normalized $Q_\infty$ for fixed resonant air-gap thicknesses $k_0 d_a = \pi - (1/\Delta\tau)$ versus normalized metal film thickness $x \equiv d_c/\delta$. The curves (from left to right) correspond to $\tau = 80, 70, 60, 50, 40, 30, 20, 10, 9, 8, 7, 6, 5, 4, 3, 2, 1$.

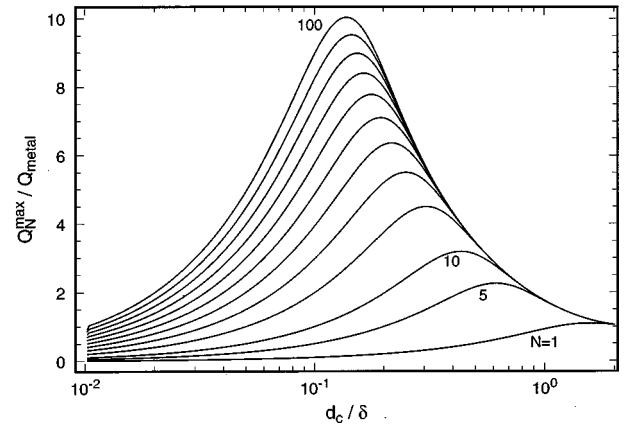


Fig. 6. Normalized maximum $Q_N$ (with continuously optimized air-gap thicknesses $y = \pi - (x^{0.9965}/\Delta)$] versus normalized metal film thickness $x \equiv d_c/\delta$.

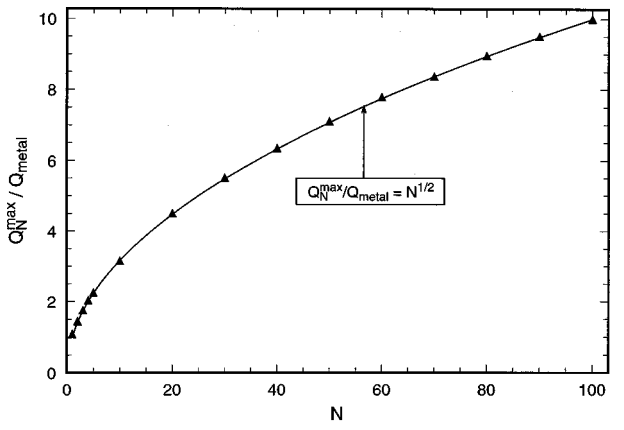


Fig. 7. Normalized $Q_N$, maximized in both $d_c$ and $d_a$, versus number of layers $N$.

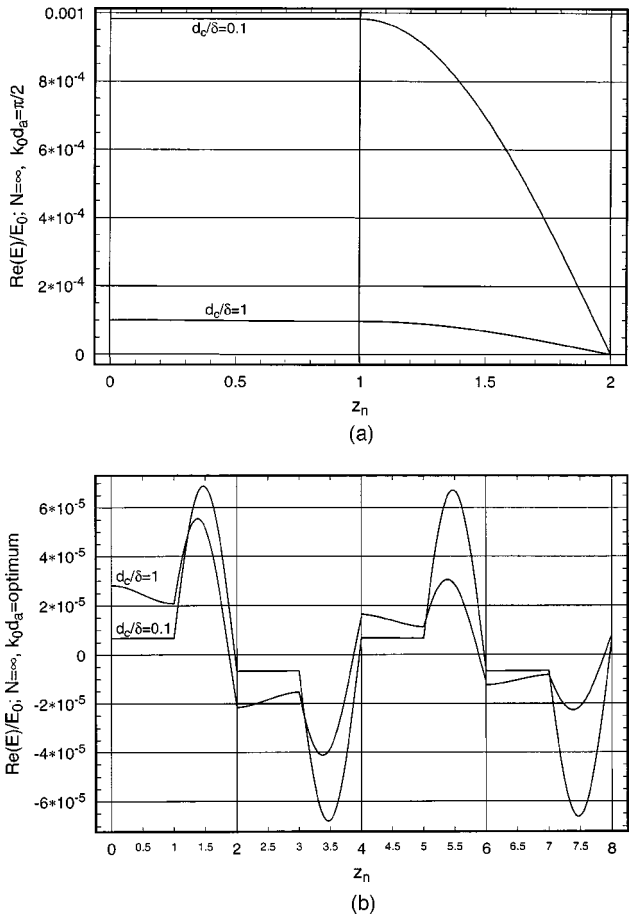


Fig. 8. Electric field distribution, normalized to incident field amplitude, inside the semi-infinite structure ($z > 0$) for normal incidence and two film thicknesses and for two air-gap thicknesses: (a) quarter-wavelength (antiresonant) and (b) optimized according to Eq. (58) for maximum reflectivity.

In Fig. 8 we show the $E$-field distribution (real part) inside the $N = \infty$ structure versus the nonlinear observation coordinate $z_n$. This coordinate expands the film thickness to allow detailed visualization of the field inside the thin metal films. It relates to actual positions on the $z > 0$ axis through the formulas ($\rho$ is any integer on the plots)

$$\begin{aligned} 2\rho < z_n < 2\rho + 1 &\rightarrow z \\ &= \rho(d_c + d_a) + (z_n - 2\rho)d_c, \\ 2\rho + 1 < z_n < 2(\rho + 1) &\rightarrow z \\ &= \rho(d_c + d_a) + d_c + (z_n - 2\rho - 1)d_a. \end{aligned} \tag{60}$$

The integers on the plots coincide with the successive air–metal interfaces ($z_n = 0 \rightarrow$ first interface of first metal film, $z_n = 1 \rightarrow$ second interface of first metal film, $z_n = 2 \rightarrow$ first interface of second metal film, etc.). We see that for nonresonant spacing [Fig. 8(a)] the field is stronger inside the metal than in the air gap (high dissipation) and, interestingly, is more so for thinner than for thicker films. On the contrary, for resonant spacing as in Fig. 8(b), the field distributes itself so that it has smaller values in the metal than in the air gap, more so for thinner than thicker films. However, the minimum possible

value in the metal film is never zero, and the nodes of the field are always in the air, close to the metal interface.

## 7. MICROWAVE-TO-OPTICAL TRANSITION

As is clear from the skin depth plots of Fig. 2 and especially from the dispersion diagrams of Fig. 3, a dramatic transition occurs in the electromagnetic response of the filter, for any number of films, as we cross the optical frequency band $\gamma < \omega < \omega_p$. This can be seen even at the well-known plasma frequency transparency transition of the bulk metal,[1] but filters will have a much more interesting response because of multiple reflection coherence effects that are superimposed on the bulk dispersion, as has been shown in Ref. 5.

### A. Optical Multiplexing

In Fig. 9 we show the filter response of an $N$-section filter for fixed conductor and air-gap thicknesses. The air gap is chosen to resonate at the plasma frequency. We see that very high transmission is possible below the plasma frequency, despite the fact that the total bulk of the metal is much larger than 1 skin depth. In fact, a four-section filter transmits 95% of the power at a frequency where the single film, with one fourth the total material, has only 70% transmittivity. This is of course due to the standing-wave effect produced by the periodicity, in conjunction with the optical properties of the bulk metal at that frequency range.

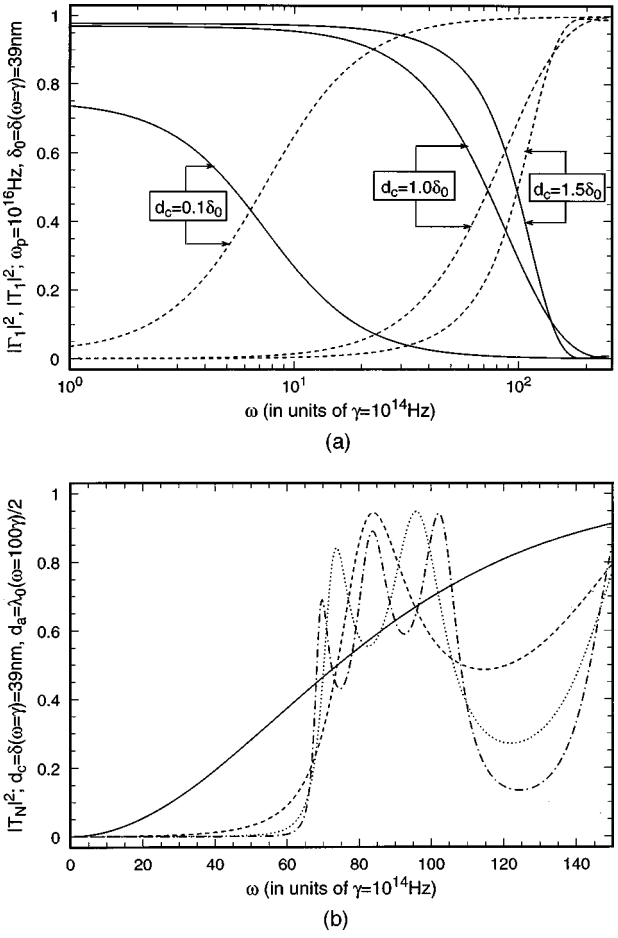


Fig. 9. (a) Reflectivity (solid curves) and transmittivity (dashed curves) of a single metal film, versus $\omega$, for various film thicknesses parameterized in terms of conductor skin depth $\delta_0$ (evaluated at $\omega = \gamma$); (b) transmittivity for fixed unit-cell thicknesses as a function of $N$ and $\omega$ for $N = 1$ (solid curve), $N = 2$ (dashed curve), $N = 3$ (dotted curve), and $N = 4$ (dotted–dashed curve).

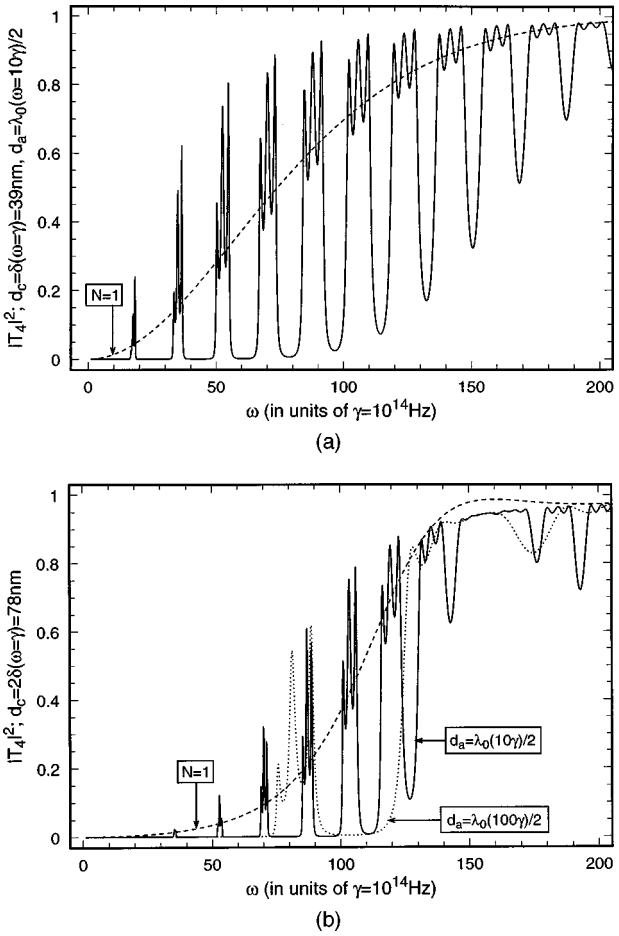


Fig. 10. Multiplexing at optical frequencies for different air (dielectric) thicknesses $d_a$: (a) for film thickness $\delta_0$ and (b) for film thickness $2\delta_0$.

In Fig. 10 we show the optical multiplexing properties of the filter. The periodicity of the response is controlled by the air (dielectric) thickness, which we normalize as a half-wavelength at parametrically chosen frequencies. However, strong dispersive effects are prominent, and the scaling of the response is not periodic. The response is that of a comb filter, but it is modulated by the transmittivity of the single metal film. Again, in the passbands the transmittivity greatly overshoots the single-film values. In particular, in Fig. 10(b) we see that the four-section filter can overshoot in transmission the single film by as much as a factor of 3, despite having four times more metal, totaling 8 skin depths. The first few stop bands, on the other hand, transmit very close to zero.

### B. Optical Mirrors

Another important issue is the performance of mirrors in the optical regime, especially at UV frequencies. In this subsection we will show the performance of the optimized filter for maximum possible reflectivity, scaled again in a

universal manner that is largely independent of the specific parameters of the metal. We will first show the maximum possible reflectivity for a semi-infinite system for various optical frequencies.

In Fig. 11 we show the maximum reflectivity of the semi-infinite system as a function of normalized metal film thickness at the plasma frequency $\omega = 100\gamma = \omega_p$, which corresponds to $\lambda = 180$ nm with our choice of parameters. The discrete points correspond to continuously optimized parameters at discrete metal thicknesses.

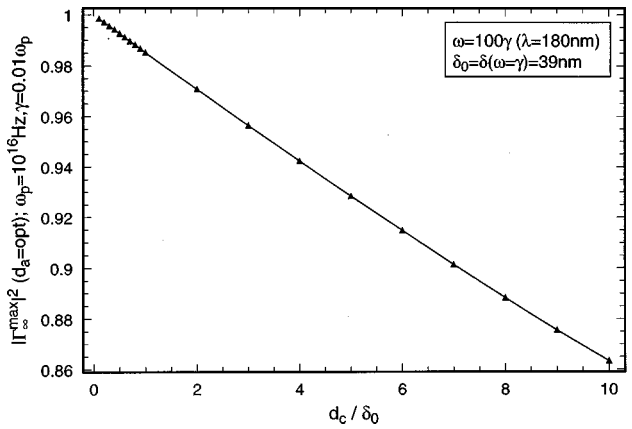


Fig. 11. Maximum reflectivity for the semi-infinite system under normal plane-wave incidence, versus normalized film thickness, at the plasma frequency (near UV).

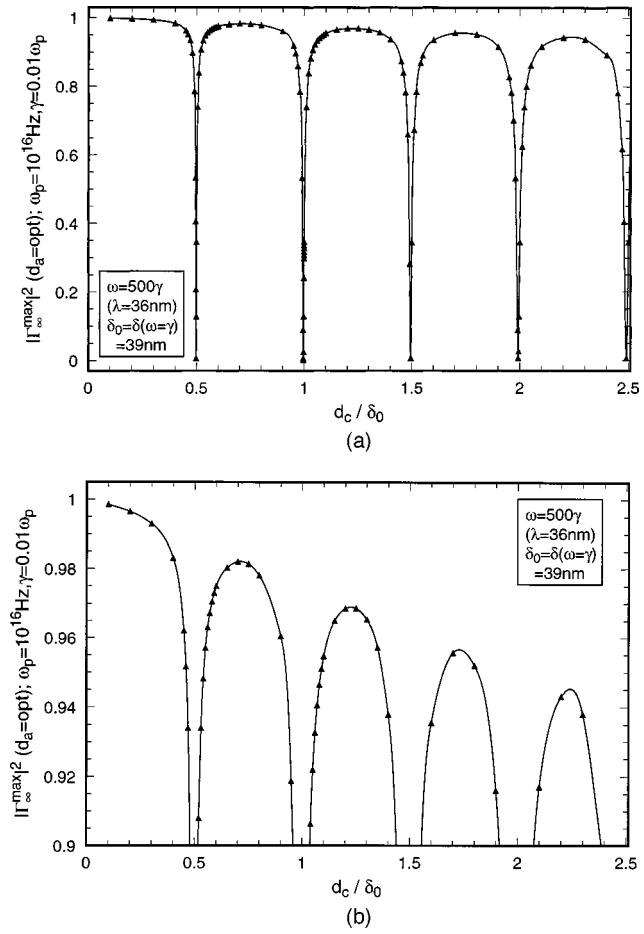


Fig. 12. Same as in Fig. 11, but at the far UV ($\omega = 5\omega_p$).

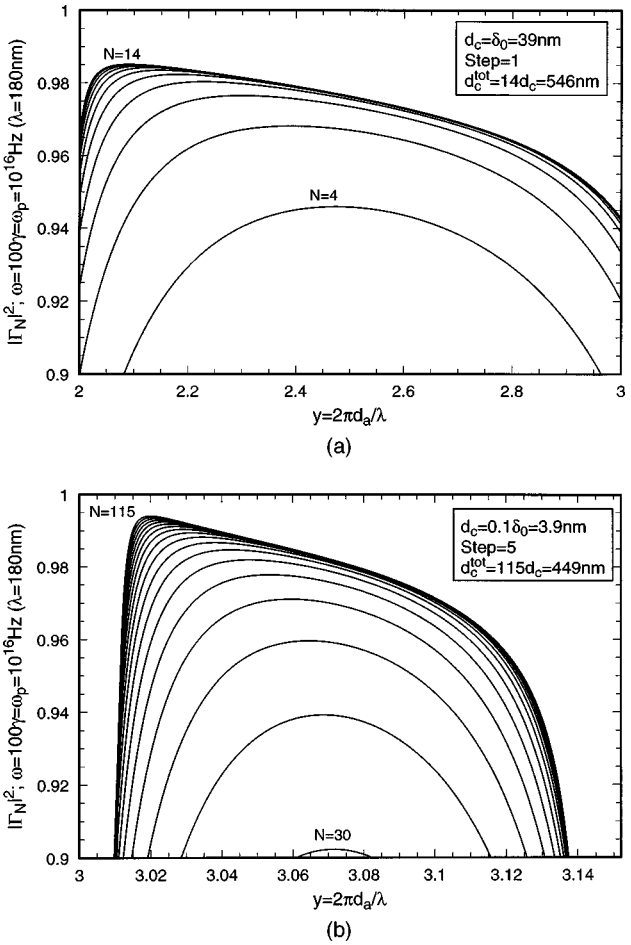


Fig. 13. Convergence of the reflectivity at resonant spacing for $\omega = \omega_p$ (corresponding to Fig. 11) and two selected thicknesses: (a) film thickness $\delta_0$ and (b) film thickness $0.1\delta_0$.

We observe that the maximum reflectivity function is quite high and is a decreasing linear function of the normalized film thickness. This was also the case at microwave frequencies, as seen from Fig. 5 and Eq. (57), if we convert the $Q$-factor normalization of that figure:

$$\frac{Q_\infty^{\max}}{Q_{\text{metal}}} = \sqrt{\pi}\frac{\delta}{d_c} \rightarrow |\Gamma_\infty^{\max}|^2 = 1 - \frac{Q_{\text{metal}}}{\sqrt{\pi}}\frac{d_c}{\delta}. \quad (61)$$

In Fig. 12 we plot the same optimized reflectivity at the extreme-UV frequency $\omega = 500\gamma = 5\omega_p$, corresponding to $\lambda = 36$ nm with our parameter choice. We see that the maximum reflectivity function now resonates in $d_c/\delta$ and varies from zero up to very high values. The high end of the reflectivity is shown in detail in Fig. 12(b). Again, the reflectivity gets larger for thinner films *but not monotonically*. Therefore it is important to avoid such film thicknesses in the mirror design, since they would ensure almost zero reflectivity no matter what the number of films.

These results are useful for specific designs of realistic mirrors containing a finite number of unit cells. The way in which the finite-$N$ system approaches the semi-infinite one is not linear in reflectivity versus film thickness.

Therefore economy of design for given reflectivity specifications is an issue that can be analyzed by plotting the response for various $N$.

In Figs. 13(a) and 13(b), we show the reflectivities of finite-section filters, as they converge to the $N = \infty$ limit, for film thicknesses $d_c = \delta_0$ and $d_c = 0.1\delta_0$, respectively, at $\omega = 100\gamma = \omega_p$. For the thicker film 14 sections essentially approach the $N = \infty$ performance (98.5% reflectivity for a total conductor thickness of 546 nm). The thinner film yields 99.5% reflectivity for 115 sections with 449-nm total conductor thickness. In Figs. 14(a) and 14(b), we show corresponding results at $\omega = 500\gamma = 5\omega_p$. The thicker film saturates the performance with 220 sections at 98% reflectivity, while the thinner film does so with 330 sections and 99.5% reflectivity.

## 8. CONCLUSIONS

In this paper we have presented a general analysis of the electromagnetic properties of planar periodic multilayers consisting of an arbitrary number of thin metallic films of arbitrary thickness. We covered a very large frequency spectrum that encompasses most engineering applications, ranging from dc to the far UV. We presented closed exact analytical formulas for the reflection and the transmission of electromagnetic waves off these structures, as well as for the Bloch–Floquet complex propagation constant of the corresponding semi-infinite multilayers. Our results were presented in appropriately scaled variables and are therefore universal, correctly scaled with respect to physical thicknesses and independent of the specific permittivity parameters of the metal. Finally, several new scaling laws in the electrodynamics of thin films were derived.

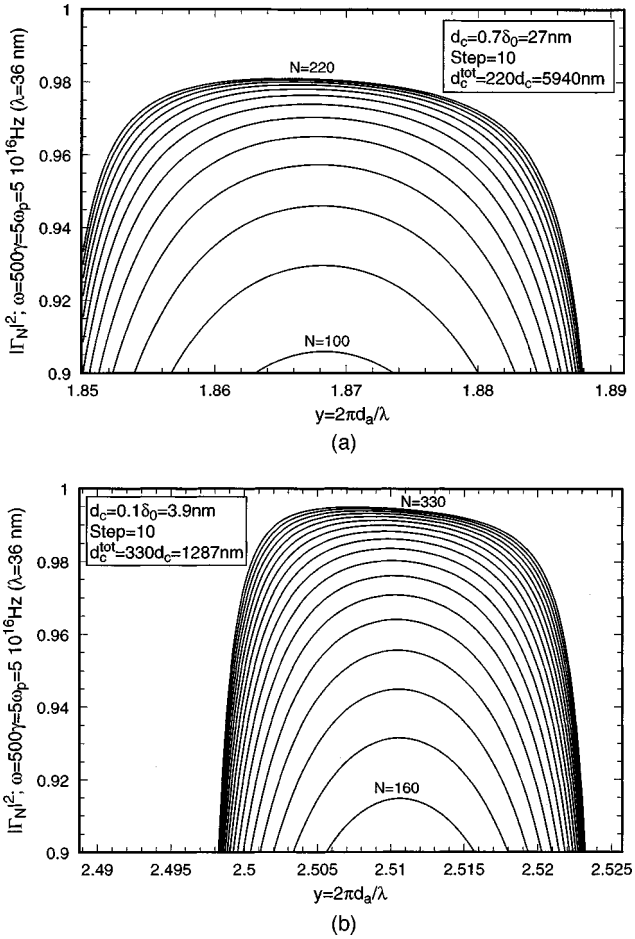


Fig. 14. Same as in Fig. 13, but at the far UV ($\omega = 5\omega_p$) and for the two selected thicknesses in Fig. 12: (a) optimum film thickness $0.7\delta_0$ and (b) film thickness $0.1\delta_0$.

First, at microwave frequencies, we pointed out that a new fundamental thickness for the metal film emerges, the impedance of free-space equivalent thickness (IFSET). This thickness is a fundamental characteristic of metals, independent of frequency and depending only on fundamental parameters of the metal permittivity. In that sense it characterizes the metal in a more fundamental way than the skin depth, which is frequency dependent. Regarding the electromagnetic properties of IFSET, it is the film thickness at which the power balance of the film has the maximum absorption and defines the film's lower thickness limit for high reflectivity.

We have further derived simple scaling laws for the maximum reflectivity of the semi-infinite and finite multilayers as a function of both film thickness and number of unit cells. At frequencies $\omega < \gamma$ the multilayer is completely opaque, and the reflectivity can overshoot the bulk reflectivity of the metal considerably. At optical frequencies the multilayer behaves as a multiplexer, with capabilities of both high transmission and high reflection. In the visible range, where single films of specific thickness can be fairly opaque, very high transmission is possible for a multilayer of such films. On the other hand, even at UV frequencies, where a single thin metal film is almost completely transparent, reflectivities of the multilayer of 99% are possible for a few hundred films.

## ACKNOWLEDGMENT

This material is based on work supported in part by the U.S. Army Research Office under contract DAAH04-96-1-0389.

Corresponding author H. Contopanagos can be reached at his present address, HRL Laboratories, 3011 Malibu Canyon Road, Malibu, Calif. 90265, or by telephone, 310-317-5487, or e-mail, contopan@hrl.com.

## REFERENCES

1. C. F. Bohren and D. R. Huffman, *Absorption and Scattering of Light by Small Particles* (Wiley, New York, 1983), Chap. 9, pp. 227–259 and references therein.
2. A. J. Ward, J. B. Pendry, and W. J. Stewart, "Photonic dispersion surfaces," J. Phys. Condens. Matter **7**, 2217–2224 (1995).
3. H. Contopanagos, N. G. Alexopoulos, and E. Yablonovitch, "High-*Q* radio frequency structures using one-dimensionally periodic metallic films," IEEE Trans. Microwave Theory Tech. **46**, 1310–1312 (1998).
4. E. Spiller, *Soft X-Ray Optics* (SPIE Optical Engineering Press, Bellingham, Wash., 1994).
5. M. Scalora, M. Bloemer, A. Manka, A. Pethel, J. Dowling, and C. Bowden, "Transparent, metallo-dielectric, one-dimensional, photonic band-gap structures," J. Appl. Phys.

**83**, 1–7 (1998); M. Bloemer and M. Scalora, "Transmissive properties of Ag/$MgF_2$ photonic band gaps," Appl. Phys. Lett. **72**, 1676–1678 (1998).
6. P. Yeh, *Optical Waves in Layered Media* (Wiley, New York, 1988), Chap. 2, pp. 128–142 and references therein.
7. M. Born and E. Wolf, *Principles of Optics*, 4th ed. (Pergamon, Oxford, UK, 1970), Chap. 1, pp. 66–70 and references therein.
8. H. Contopanagos, N. Alexopoulos, and E. Yablonovitch, "High-*Q* rectangular cavities and waveguide filters using periodic metalo-dielectric slabs," in *IEEE Microwave Theory and Techniques International Microwave Symposium Digest*, June 7–12, 1998 (Institute of Electrical and Electronics Engineers, New York, 1998), pp. 1539–1542.
9. H. Ehrenreich and H. R. Philipp, "Optical properties of Ag and Cu," Phys. Rev. **128**, 1622–1629 (1962); H. Ehrenreich, H. R. Philipp, and B. Segall, "Optical properties of aluminum," Phys. Rev. **132**, 1918–1928 (1963).
10. E. Yablonovitch, "Photonic band-gap structures," J. Opt. Soc. Am. B **10**, 283–295 (1993); C. M. Soukoulis, ed., *Photonic Band Gaps*, Vol. 315 of NATO ASI Series E (Kluwer Academic, Dordrecht, The Netherlands, 1996).
11. A. E. Kaplan, "On the reflectivity of metallic films at microwave and radio frequencies," Radio Eng. Electron. Phys. **9**, 1476–1481 (1964).